Global NEST Journal, Vol 25, No X, pp 1-10

Adsorption of Co(II) ions using indigenous tamarind seed biochar: batch adsorption and modeling studies

Gomathy B.L.J.[1], Karthik V.[2*] and Periyasamy S.[3]

[1]Department of Electronics and Instrumentation Engineering, Government College of Technology, Coimbatore–641013, Tamil Nadu, India

[2]Department of Industrial Biotechnology, Government College of Technology, Coimbatore–641013, Tamil Nadu, India

[3]Department of Chemical Engineering, School of Mechanical, Chemical, and Materials Engineering, Adama Science and Technology University, 1888 Adama, Ethiopia

Received: 03/04/2023, Accepted: 02/05/2023, Available online: 27/05/2023

*to whom all correspondence should be addressed: e-mail: karthikbt88@gmail.com

https://doi.org/10.30955/gnj.005046

Graphical abstract

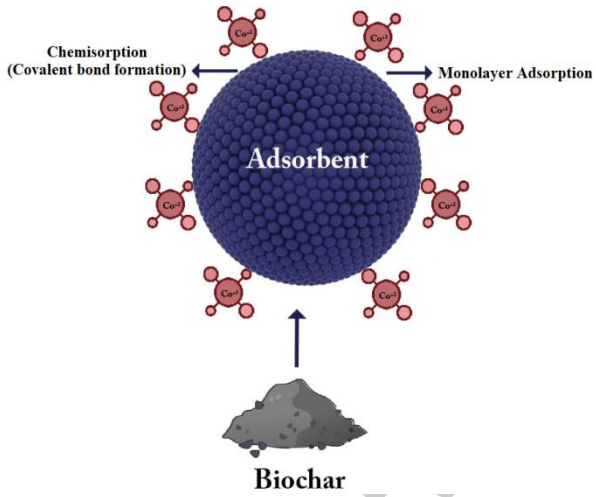

Abstract

With an estimated volume of 162 thousand metric tonnes in 2020, India is the world's largest producer of tamarind. The country is home to a number of tamarind species, and production is spread out across the country. Farmers and agro-industries continue to encounter numerous challenges in the processing and disposal of waste created during tamarind harvesting and processing. However, because this agricultural waste is disposed of fast, it may pollute the ecosystem. As a result, this study focused on agricultural waste reuse for wastewater treatment, with tamarind seeds serving as the principal source for low-cost adsorbent (biochar) manufacture to remove harmful Co (II) ions rendered as an aqueous solution. Biochar is a form of charcoal produced by the pyrolysis of organic materials such as wood, agricultural waste, and animal manure. The surface characteristics of the synthesized biochar from tamarind seeds were investigated using FTIR spectroscopy, XRD, SEM, and EDAX. Tamarind seeds-based biochar (TSB) achieves maximal Co (II) ion adsorption at 9 pH, 50 °C, 90 min contact period, and 0.14 g/L adsorbent dosage. The Langmuir isotherm and Pseudo-second-order kinetics are the best-fitting isotherms and models for Co (II) ion adsorption using TSB. The maximal monolayer adsorption capacity (q_m) of tamarind seeds-based biochar was determined by an adsorption isotherm analysis of 343.5 mg/g for Co (II) ions. Thermodynamic parameters successfully indicate that the current Co (II) ion adsorption utilizing TSB is possible, spontaneous, and endothermic. As a result, the adsorption investigation demonstrates that generated TSB has improved surface characteristics and capacity to remove Co (II) ions from wastewater effectively.

Keywords: Agricultural waste, tamarind seeds, biochar, waste re-utilization, Co(II) ions, adsorption

1. Introduction

Heavy metals, dyes, pharmaceuticals, pesticides, herbicides, and radioactive pollutants are all found in wastewater produced by various manufacturing and processing industries (Karthik *et al*., 2022a). These primary pollution sources affect the environment, specifically water pollution. To avoid many environmental issues and health-related problems for humans, aquatic animals, and plants, wastewater must be treated before it is released and infused into a natural water resource (Obaideen *et al*., 2022, Sikiru *et al*., 2022). Heavy metals are significant environmental pollutants discharged directly into water resources from various manufacturing and processing industries, including mining, paint, textile, metal-plating, petrochemical plants, oil refineries, pesticide, and other chemical production (Velusamy *et al*., 2022). Arsenic, cobalt, lead, mercury, cadmium, nickel, and chromium are the most often used heavy metals in critical industries that could contaminate the environment (Ekrami *et al*., 2022). However, some metal ions, such as copper, molybdenum, chlorine, zinc, magnesium, nickel, and cobalt, are required as micronutrients for plants and animals in the environment. They may have toxic and harmful effects if they exceed specific concentrations

known as the maximum permissible limit (Akshitha *et al*., 2022, Sithara *et al*., 2017).

Cobalt is a heavy metal commonly used in manufacturing and processing, including battery, electroplating, textile, and glass (Abdelbasir *et al*., 2021, Güçoğlu and Şatıroğlu, 2022). Cobalt exists primarily in the +2-oxidation state (Co(II) ions) as opposed to the other oxidation states ranging from -3 to +5. However, while Co(II) ions have potential beneficial applications in various industries, they have several adverse effects when discharged into water resources as wastewater. Inhaling and ingesting Co(II) ions causes various adverse health effects in humans, including coughing, congestion in the chest, wheeziness, respiratory distress, asthmatic attack, heart disease, and interference with the function of the liver, bone marrow, kidneys, and thyroid (Leyssens *et al*., 2017, Zhu *et al*., 2021, Al-Abcha *et al*., 2021, Teschke, 2022). As a result, removing Co(II) ions from contaminated water/wastewater is critical and safe for humans and other organisms in the ecosystems.

Wastewater treatment is one of the evolving domains in which many researchers are still working to develop suitable solutions to eliminate pollution while preserving the natural attributes of the environment (Asaithambi *et al*., 2020, Rajesh Banu *et al*., 2021, Karthik *et al*., 2021). For wastewater treatment, various conventional technologies include ion exchange, precipitation, filtration, membrane separations, floatation, electrocoagulation, and other electrochemical treatments were already used (Velusamy *et al*., 2021a, Asaithambi *et al*., 2021, Karthik *et al*., 2022b). Adsorption is the most successful and affordable of these approaches (Wang *et al*., 2021, Velusamy *et al*., 2021b). Despite being used for decades, these methodologies have challenges in various areas making these processes unsuitable for implementation and operation (Periyasamy *et al*., 2022, Murugesan *et al*., 2022). Compared to more conventional procedures, adsorption is among the most efficient, widely applicable, and feasible options. However, conventional materials, such as commercial activated carbons used as adsorbents for wastewater treatment, are more expensive, and the process is more effective than other conventional approaches. Because the cost of adsorbent material prevents pilot-scale implementation, many researchers have recently developed a variety of alternatives, including waste-based adsorbents for effective removal comparable to conventional adsorbents (Roba *et al*., 2023). Some of the waste-based adsorbents that have recently been developed and used as adsorbents for wastewater treatment include recycled electrical circuit boards, various carbon materials, plant waste-based nanomaterials, vegetable wastes, fruit wastes, sawdust, clay-based materials, agricultural wastes such as sugarcane molasses, beet molasses, tea and coffee wastes, almond, tamarind seeds, peanut, and walnut shells, lotus stalk, rice straw, wheat bran, and rice (Shrivastava and Singh, 2022, Silva *et al*., 2018, Agarwal and Singh, 2017).

Biological components of agricultural waste, such as carbohydrates, proteins, and lipids, are responsible for improved surface properties and a plethora of required functional groups, critical in the adsorption of harmful pollutants (Periyasamy *et al*., 2023). Because agricultural waste has effective surface properties for the adsorption of various toxic contaminants, their surface properties were enhanced by various surface modification processes such as acid treatment, alkali treatment, carbonization, gasification, thermal processes including pyrolysis, microwave-assisted, and chemical activations to increase their effectiveness and stability for continuous wastewater treatment (Azam *et al*., 2022). Tamarind seeds are one of the most common wastes generated during tamarind processing in cumbersome volumes from an agricultural process. The authors tested the efficacy of TSB for removing Cr, Pb, and Cd from simulated wastewater in their study. The study discovered that TSB was effective for heavy metal removal, with up to a 99.5% removal efficiency for Pb and up to 94% for Cr and Cd. The authors also discovered that the adsorption capacity of TSB increased as metal concentrations increased, indicating that TSB is a promising adsorbent for heavy metal removal from contaminated waters.

Bhairappa *et al*. investigated the potential of TSB for the adsorption of Cu, Zn, and Pb from the soil in a follow-up study. The authors discovered that TSB was effective for heavy metal removal, with up to a 97% removal efficiency for Cu and up to a 95% removal efficiency for Zn and Pb. The authors also discovered that the adsorption capacity of TSB increased with increasing metal concentrations, implying that TSB could be a useful adsorbent for heavy metal removal from soil. The authors also discovered that the adsorption capacity of TSB increased as metal concentrations increased, indicating that TSB is a promising adsorbent for heavy metal removal from industrial wastewater.

The current study is concerned with treating Co(II) contaminated wastewater using an economically viable and effective adsorption approach. The adsorbent and its characteristics are the cardinal constituents in wastewater treatment adsorption. This study's primary source for adsorbent (biochar) preparation was tamarind seeds, an abundant agricultural waste material. Pyrolysis was used to create effective surface properties-rich biochar from tamarind seeds. The surface properties of biochar that lead to adequate Co(II) ion adsorption were evaluated using characterization studies such as FTIR and XRD analysis. The parameters influencing Co(II) ion adsorption-based exclusion from the metal ion dissolved solution were optimized using batch adsorption studies. Eventually, adsorption isotherm and kinetic modeling studies were done to figure out Co(II) ions adsorption to biochar made from tamarind seeds. The thermodynamic study also explained the possible action patterns for Co(II) ions adsorption to biochar made from tamarind seeds.

2. Experimental methods and preparations

2.1. Biochar preparation

Before being placed in porcelain crucibles with covers, the collected tamarind seeds were cleaned with deionized

water and sun-dried. The collected samples are pyrolyzed in an oxygen-deficient muffle furnace at approximately 400 °C at a 20 °C min^{-1} heating rate. Biochar is then centrifuged to remove the ash content before being treated (100 °C) in a hot air oven for drying. A mortar and pestle were used to obtain the powdered form of biochar. The collected biochar was maintained in an airtight container for all further analyses.

2.2. Characterization of adsorbent

The Fourier Transform Infrared Spectroscopy (FTIR) (8400SSHIMADZU, Japan) instrument was used to record the infrared spectrum of the synthesized adsorbent before and after adsorption. To identify functional and structural changes in adsorbents, they have transformed into Potassium bromide (KBr) pellets and scanned from 4000 to 400 cm^{-1} with 4 cm^{-1} resolution against a blank Potassium bromide pellet. The nature of molecules and their atomic structure could be deduced by analyzing the adsorbent's X-ray diffraction (XRD) patterns. XRD spectrogram aids in identifying the crystalline phase of the adsorbent concerning adsorption. The patterns are generated using the D8 Advance ECO XRD systems with a detector (SSD160 1 D-BRUKER). RFB-400 is referred to as the control in sorption. Adsorbent before and after adsorption processes were studied using scanning electron microscopy (SEM) and energy dispersive x-ray spectroscopy (EDAX) (SIGMA HV – Carl Zeiss with Bruker Quantax 200 – Z10 EDS Detector). A study on the topographical characteristics would provide the nature of adsorption and structural changes in the surface of the adsorbent. SEM and EDX were employed to determine the elemental distribution of biochar composites at the surface and near the surface.

2.3. Preparation of Co (II) solution

Stock solution for adsorption studies was prepared with $CoCl_2.6H_20$ in deionized water at 1 g/L of Co(II) ions concentration. A working solution was prepared from the Co(II) stock solution with deionized water at various concentrations.

2.4. Adsorption studies

The pH of the working Co(II) solution was adjusted to 9 and 4 with 0.5 M NaOH and 0.5 M HCl. After adding 100 mg of adsorbent (Biochar) to 50 mL of each Co (II) solution, the flask was closed and kept in a rotary shaker at 150 rpm for 90 minutes. The adsorbent metal solution was filtered after a specified period to measure the solution concentration after adsorption. The optical density with a UV-Vis spectrometer was recorded for the filtrate, and the adsorption efficiency was calculated. The adsorption efficiency was measured for different experimental factors, including pH, initial metal ion concentration, contact time, and working temperature at regular intervals. The percentage removal of metal could be calculated from

$$\% \text{ Removal} = \frac{C_i - C_0}{C_i} \times 100 \quad (1)$$

C_i is the initial, and C_0 (mg L^{-1}) is the solution's final metal concentration. At any time, t, metal adsorption capacity q_t (mg/g) is calculated from

$$q_t = (C_i - C_t) \times \frac{V}{M} \quad (2)$$

V (L) denotes the volume of the metal solution, C_t (mg/L) is the metal ion concentration at any time, and M (g) is the quantity of TSB.

3. Results and discussion

3.1. Physiochemical characterization of adsorbent

Many different characterization approaches, including FTIR, XRD, and SEM, were used to examine the qualities of the TSB adsorbent.

3.1.1. Infrared spectra analysis

FTIR employs infrared light as its primary illumination source to identify organic polymeric and inorganic materials. The FTIR spectra obtained before and after the adsorption of Co(II) ions showed significant changes in the adsorption pattern, indicating that the chemical structure of the biochar was modified after the adsorption process. The changes in the adsorption bands provide evidence of a transformation in the chemical construct of the material. TSB was used to remove Co(II) ions, and the adsorbent's spectra were obtained before and after the adsorption process. After adsorption, the biochar contains many different functional group modifications, as indicated by the multiple peaks with varying transmittance compared to the adsorbent before adsorption (Figure 1). For example, the strong C-H bending at 823 cm^{-1} suggests the presence of aliphatic or aromatic hydrocarbons, which may have been introduced by the adsorbed Co(II) ions. The C-O stretching at 1220 cm^{-1} indicates the presence of carboxylic acid or ester groups, which may have been formed due to the interaction between the biochar and Co(II) ions. Moreover, the C=O stretching of the carboxylic acid dimer that can be seen at 1742 cm^{-1} in the IR spectra of biochar following adsorption shows the existence of new functional groups on the biochar surface.

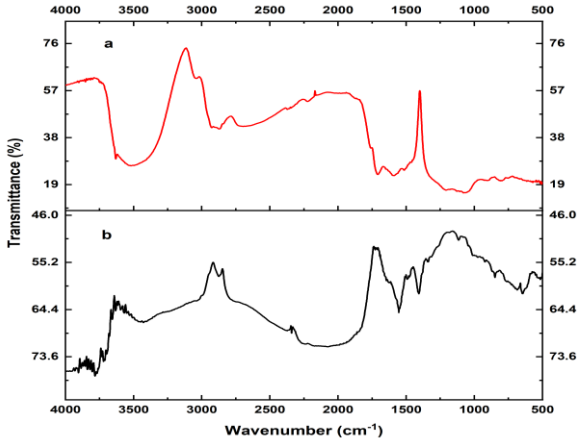

Figure 1. Fourier spectral analysis for TSB (a) before and (b) after adsorption

Furthermore, the major functional groups in TSB include a mild C-H stretching aldehyde doublet at 2732 cm^{-1}, an alkane C-H stretch at 2915 cm^{-1}, and sharp alcohol-free O-H stretching at 3632 cm^{-1} and 3980 cm^{-1}. The biochar's most significant peak would be for C-O stretching, with C=O stretching detected at 1350 cm^{-1} to 1420 cm^{-1} and bend at 540 cm^{-1} to 650 cm^{-1} (Hossain *et al*., 2020). The modified peaks obtained after the adsorption process display the functional breakdown of the functional groups. The changes in the significant peaks that correspond to pure biochar demonstrate chemical modification after adsorption. The interaction of Co (II) with functionally available carboxyl units on the biochar surface could contribute to the disbandment of these functional groups. This change to carboxylates demonstrates the critical function that the carboxyl groups of the adsorbent play in metal binding (Medyńska-Juraszek *et al*., 2020).The changes in the adsorbent's peaks at 3464 cm^{-1} and 3632 cm^{-1} suggest that OH was involved in the complexation of Co (II) to the biochar. The metal ion could have spiked the characteristic peak of the adsorbent with decreased intensity (Papageorgiou *et al*., 2010). The overall spectral trend and the peak difference in FTIR spectral reflectance after adsorption indicates functional and structural modifications caused by Co(II) adsorption to the synthesized adsorbent.Because of adsorption, the transmission percentage for each functional class is decreased, which suggests that Co(II) ions were effectively adsorbed onto TSB.

3.1.2. XRD analysis

XRD analysis investigated the crystalline structure of modified biochar, and the findings are shown in Figure 2. The Debye - Scherrer equation is often used to determine the mean crystallite size,

$$d = \frac{0.9\lambda}{\beta \cos\theta} \quad (3)$$

d is the crystal grain size, θ is the angle of reflection, ʎ is the wavelength used, and β is the full width at half the maximum of the diffraction line broadening

The XRD (X-ray diffraction) patterns of biochar both before and after the adsorption of metal ions, more especially Co, are depicted in Figure 2. Strong peaks can be seen in the XRD pattern of biochar before it has been subjected to adsorption. These peaks are located at 28°, 41°, 52°, and 66.5°, and they correspond to various materials such as $AlFeO_3$, Fe_2O_3, $FeAlO_3$, and Al_2O_3, respectively. In addition, there is a large diffraction peak at 2θ values of 28.4°, demonstrating that carbon is an amorphous material(Shi *et al*., 2019). The XRD pattern shows that biochar is amorphous, which is corroborated by the fact that there are fewer peaks. Moreover, the peaks that are there are smaller. After adsorption, the XRD pattern of the biochar demonstrates an increase in intensity at the adsorbent site, which indicates successful adsorption. In addition, several additional peaks manifest, which can be attributed to the interaction between the metal ions and the adsorbent. As an outcome of this interaction, the crystallinity of the adsorbent undergoes a very minor change. The discovery of additional peaks following adsorption adds credence to the idea that the surface of the biochar has undergone structural modifications due to its interaction with metal ions. Also, the appearance of peaks that correspond to Co(II) in the XRD pattern of the biochar following adsorption provides further evidence that Co(II) was successfully adsorbed on the surface of the biochar. Because these peaks were absent before adsorption, it may be deduced that the biochar did not originally consist of Co(II). Because of this, the XRD pattern proves that metal ions, notably Co(II), were successfully adsorbed onto the surface of the biochar. The XRD pattern taken before adsorption shows that the biochar is amorphous. On the other hand, the XRD pattern has taken after adsorption shows successful Co(II) adsorption on the surface of the biochar, effective adsorption, and a shift in the crystallinity of the adsorbent.

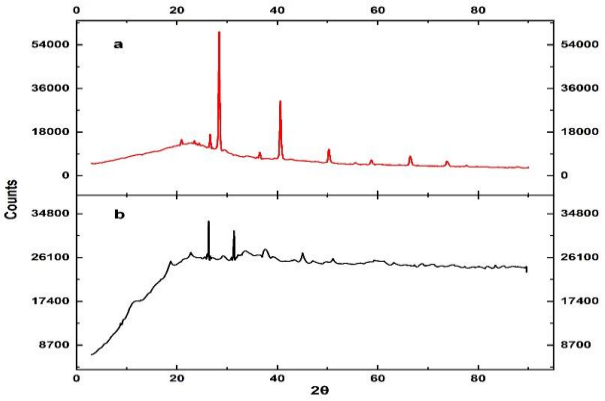

Figure 2. XRD analysis result of TSB (a) before and (b) after adsorption

3.1.3. SEM and EDAX analysis

SEM study of the adsorbent's topographical structure before and after Co (II) adsorption at 10 kV is shown in Figure 3. The adsorbent's surface was examined using SEM, and numerous carbon particles were observed due to pyrolysis (Huang *et al*., 2016). After adsorption, the adsorbent's surface showed rugged aggregates, indicating the interaction between the metal ion and the adsorbent. The adsorbent surface also displayed porous structures, which could enhance the surface adsorption of the metal ion. The breakdown of cellulose, hemicellulose, and other components during high-temperature pyrolysis could have formed these porous structures and numerous carbonized particles (Wu *et al*., 2019).

Additionally, the elemental analysis of the adsorbent was carried out using EDAX, and Co (II) ions were found in the adsorbent spectrum after adsorption. The presence of Co (II) ions suggested that the metal ion had interacted with the adsorbent surface and resulted in binding for complex formation. The adsorbent spectrum also revealed the presence of other elements, such as Si, O, K, Cl, and N, which resulted from pyrolysis (Chen *et al*., 2016). The overall trend of SEM and EDAX analysis demonstrated that the metal ion bound to the surface of the biochar adsorbent made from tamarind seeds due to adsorption,

and this interaction altered the topographical structure of the adsorbent slightly. The porous structures and numerous carbonized particles on the adsorbent surface could enhance the surface adsorption of the metal ion.

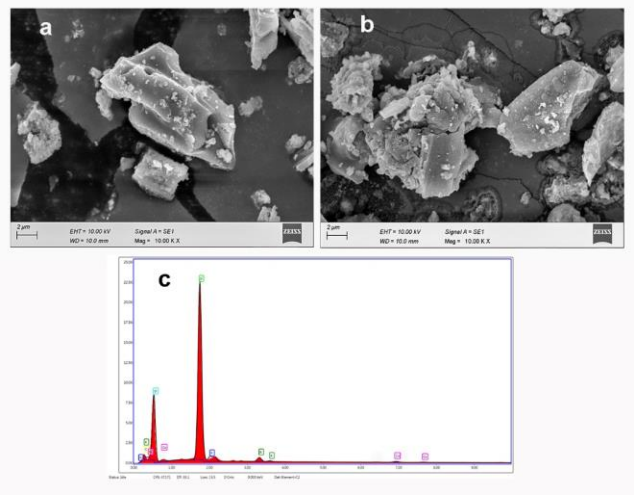

Figure 3. SEM images of TSB (a) before and (b) after adsorption, and (c) EDAX profile of the adsorbent after the adsorption

3.2. Effect of parameters on Co(II) adsorption

3.2.1. pH effect on adsorption

The process of removing heavy metals from a solution by adsorption is highly dependent on the pH of the solution. The solution's pH is an important characteristic that plays a role in controlling the rate at which the adsorption process will work. The pH level affects both the surface charge of the adsorbent and the speciation of the adsorbate that it is removing (Kılıc *et al*., 2013). According to the findings of several studies, one of the most important aspects to consider when managing the adsorption process is the solution's pH (Chen *et al*., 2016). The experiment was carried out with a biochar contact period of 75 min^{-1} utilizing 50 mg of biochar. The findings demonstrated a decline in the effectiveness of cobalt removal when the pH increased from 9 to 14, as shown in Figure 4a. Almost 99% of the total adsorption capacity was reached when the pH was 9. Nevertheless, when the pH of the solution increased beyond 9, heavy metal ion precipitation in the form of hydroxides caused the cobalt removal efficiency to decline. This was because cobalt was being removed, which suggests that the adsorption rate will decrease at lower pH levels because the biochar surface has more H+ ions that can compete with each other. These H^+ ions induce electrostatic repulsion, lowering the adsorption process's effectiveness. Moreover, they cause the Co(II) ions to be repelled.

3.2.2. Temperature effect on adsorption

The effect of temperature on the adsorption process, especially when it comes to the determination of whether or whether the reaction is endothermic or exothermic. The equilibrium capacity of the adsorbent plays a significant role in the efficiency of the adsorption process, and temperature can impact that capacity (Shen *et al*., 2019). The research was conducted using an initial concentration of 0.15 g L^{-1} at a pH of 9 utilizing 50 mg TSB, and the temperature range was evaluated from 20 to 50 °C. According to the findings, the proportion of removed cobalt grew as the temperature increased, with the highest removal rate at about 95%. Figure 4b depicts this association between an increase in temperature and an increase in adsorption efficiency. Because the adsorption process is endothermic, the capacity for absorbing Co (II) ions has increased, which may be linked to the nature of the process. Understanding the influence of temperature on the adsorption process is important since it can considerably impact adsorption efficiency (Bordoloi *et al*., 2017).

3.2.3. Initial metal ions concentration and contact time effect on adsorption

In this study, we looked at how the initial concentration of metal ions affected the adsorption of cobalt ions onto TSB, which was used as the adsorbent. The amount of Co (II) ions in the solution was raised from 50 to 250 mg/L, and the adsorption process was watched closely as it progressed over time. The findings were provided as a picture that illustrated how the elimination of Co(II) ions evolved during the study. According to Figure 4c, the amount of Co (II) ions that were removed first grew for up to 90 minutes until reaching a point of saturation after equilibrium circumstances were reached. This leads one to believe that the adsorption process was originally quite effective; however, when the adsorbent sites were filled up, the adsorption rate slowed down. However, despite this saturation effect, the adsorption capacity of the biochar-made tamarind seeds improved from 89% to 99% when the initial metal ion concentration rose. This suggests that elevating the initial concentration of Co (II) ions improved the biochar's overall adsorption effectiveness. These findings suggest that this improvement is due to more adsorption sites on the surface of the TSB. These additional sites allowed for the initial quick adsorption of Co (II) ions and contributed to the overall increase in adsorption capacity (Saravanan *et al*., 2021). TSB is a useful adsorbent for Co (II) ions, and its performance may be improved by raising the initial metal ion concentration.

3.2.4. Adsorbent dosage effect on adsorption

Using biochar as an adsorbent, an investigation was conducted to determine how the adsorbent dose affected the removal of Co (II) ions. This work investigated and analyzed the ideal amount of adsorbent necessary to achieve maximal removal of Co (II) ions. In order to provide the most favorable conditions for the experiment, they adjusted the concentrations and the adsorption dosage at an optimum pH level, which was 9. According to the findings, the best removal performance was achieved when 0.1 g of adsorbent was utilized in conjunction with a solution containing 100 parts per million Co(II) ions. The adsorbent dose steadily rose from 0.02 to 0.14 g, and the percentage removal efficiency gradually rose from 50.1% to 95.2%, as indicated in Figure 4d. This suggests that the adsorption of Co(II) ions is proportional to the increasing adsorbent dosage. This is because raising the dose of the adsorbent likewise increases the number of active sites on

the biochar adsorption. This makes it possible for more Co (II) ions to be adsorbed onto the surface of the biochar, which ultimately results in a better removal efficiency (Kılıc *et al*., 2013). These results imply that the best adsorbent dose for removing Co (II) ions from water using biochar as an adsorbent is 0.14 g. The removal efficiency may be improved by increasing the adsorbent dose, and this can be due to the increase in the number of active sites accessible for adsorption on the surface of the biochar (Karthik *et al*., 2020).

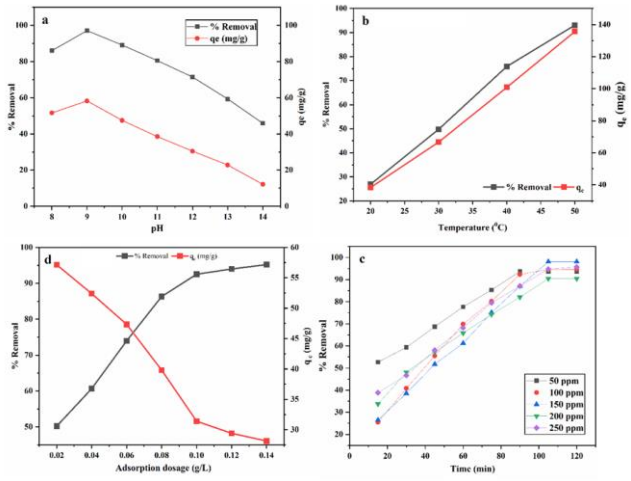

Figure 4. Effect of parameters on TSB biochar (a) effect of pH, (b) effect of temperature, (c) effect of initial concentration, and (d) effect of adsorbent dosage

3.3. Adsorption isotherm

3.3.1. Freundlich isotherm

According to the Freundlich isotherm study, adsorption occurs on a heterogeneous surface with non-uniform adsorption energy (Karthik *et al*., 2020). The Freundlich isotherm non linear equation is as follows:

$$q_e = K_f C_e^{1/n} \quad (4)$$

Where n is the adsorption intensity, and K_f is the Freundlich isotherm constant (mg/g). Figure 5 shows the measured value of Co (II) ions for the Freundlich isotherm. Table 1 shows that the Freundlich isotherm R^2 values range from 0.9162 -0.9336. The calculated evaluation of n in Freundlich isotherm was from 1.725 -2.109. Using the correlation factor, Freundlich isotherm is not well-fitted compared to the Langmuir isotherm.

3.3.2. Langmuir isotherm

Based on the Langmuir isotherm, adsorption occurs on a monolayer surface with the same energy on all adsorption sites. The adsorption isotherm provides the constants and equilibrium adsorption capacity whose values show the surface characteristics and adsorbents affinity (Karthik *et al*., 2020). The Langmuir isotherm's non-linear equation is

$$q_e = \frac{q_m K_L C_e}{1 + K_L C_e} \quad (5)$$

K_L is the Langmuir isotherm constant (L/mg), and q_m is the maximum monolayer capacity (mg/g). q_e vs. Ce were plotted with different temperatures (20, 30, 40, and 50 °C), from which K_L and q_m values were calculated (Figure 5). Table 1 shows that the q_m and K_L values rise as the temperature rises, with R^2 values from 0.9765 to 0.9852. The higher R^2 value of Langmuir isotherm shows that the Co(II) ions adsorption using TSB is best fitted with the Langmuir isotherm model than others (Saravanan *et al*., 2021).

Table 1. Isotherm constants for adsorption of Co(II) with TSB

Isotherm model	Parameters	Temperature (K)			
		293	**303**	**313**	**323**
Langmuir	q_m (mg/g)	262.1	272.9	285	343.5
	K_L (L/mg)	0.0432	0.04609	0.0507	0.04415
	R^2	0.9765	0.9823	0.9842	0.9852
	SSE	3.12	2.52	2.42	2.39
	RMSE	2.182	1.175	0.995	0.987
Freundlich	K_F ((mg/g)(L/mg)$^{(1/n)}$)	27.68	28.83	30.7	27.17
	n (g/L)	2.109	2.065	2.026	1.725
	R^2	0.9168	0.9433	0.9537	0.9936
	SSE	7.07	6.981	6.554	3.602
	RMSE	5.211	4.84	4.61	2.128
Temkin	A_T (L/g)	0.3821	0.4679	0.5411	0.6444
	B (J/mol)	26.2	25.8	26.4	27.62
	R^2	0.9721	0.9702	0.9698	0.9508
	SSE	3.728	4.23	4.644	6.157
	RMSE	2.579	3.29	3.44	4.95

3.3.3. Temkin isotherm

Based on the Temkin equation 6, the adsorption temperature in all molecules falls linearly as the surface area of the adsorbent increase (Ref will be added). The following equation can represent the Temkin isotherm.

$$q_e = \frac{RT}{b} \ln(A_T C_e) \quad (6)$$

where R is the universal gas constant (8.314 J/mol/K), A_T is the Temkin isotherm equilibrium binding constant (L/g), B is the constant related to the heat of adsorption (J/mol),

and is the temperature at 298 K**.** The plot of q_e vs. C_e at various temperatures ranging from 20 – 50 °C was shown in the figure. The A_T and B values increase when the temperature rises. The R^2 values were 0.9508 to 0.9721 (Table 1), indicating a nominal value lesser than the Langmuir isotherm. Thus, the TSB does not fit Temkin isotherm (Saravanan *et al*., 2021).

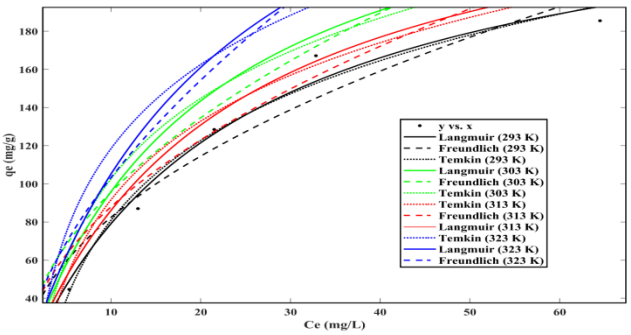

Figure 5. Isotherm of Co(II) ions adsorbent on TSB

3.4. Adsorption kinetics

3.4.1. Pseudo-first order kinetics

For lower solute concentrations, the pseudo-first-order kinetic model is more appropriate (Saravanan *et al*., 2021). The pseudo-first-order kinetic model equation is as follows:

$$q_t = q_e(1-\exp(-k_1 t)) \quad (7)$$

Figure 6 shows a plot of q_t versus t, where k_1 is the rate constant of first-order adsorption (min^{-1}). The figure indicates that the adsorption of Co (II) ions by TSB follows first-order kinetics, with the (R^2) correlation factor ranging from 0.9439 to 0.9794, indicating that the biochar can adsorb Co (II) ions even at low concentrations and that the interaction must be in monolayer adsorption.

3.4.2. Pseudo–second–order kinetics

The pseudo-second-order model is based on chemisorption and involves electrostatic forces and valence via electron sharing between the adsorbent and metal ions (Saravanan *et al*., 2021). The following formula provides this.

$$q_t = (q_e^2 k_2 t)/(1+q_e k_2 t) \quad (8)$$

Where the rate constant is k_2, the plot of q_t vs. t gives the pseudo-second-order model. Table 2 shows the values of q_e and k_2 for Co(II) ions at four different temperatures. From Figure 6, the pseudo-second-order equation fits with the experiment's data at the higher correlation coefficient (R^2) range between 0.9713 to 0.9841. It is well fitted with the pseudo-second-order kinetics model as the R^2 values are close to unity. The batch adsorption process depends on the concentration of TSB and Co(II) ions. This is a chemically rate-controlled adsorption mechanism. Then it concludes that the adsorption process is chemisorption.

3.4.3. Bangham kinetic model

Bangham's pore distribution model can help calculate the rate-controlling step in the adsorption process (Karthik *et al*., 2020), as shown in the equation below:

$$q_t = k_r t^{\frac{1}{m}} \quad (9)$$

The plot of q_t vs. t gives the Bangham kinetic model. The graph was plotted for a 150mg/L of Co(II) ions concentration, as shown in Figure 6. The plot of q_t vs. t gives the Bangham kinetic model. The graph was plotted for a 150mg/L of Co(II) ions concentration, as shown in Figure 6a. The constant values are presented in Table 2. The correlation coefficients (R^2) for Co(II) ion adsorption ranged from 0.9151 to 0.9828. The values of R^2 indicate the rate-limiting step of adsorbate diffusion into the pore or matrix for Co(II) ions. The Co(II) ions were well diffused into the adsorbent.

3.4.4. Intraparticle diffusion

Intraparticle diffusion, usually the rate-limiting stage in adsorption, transports metal ions from the bulk fluid into the adsorbent (Saravanan *et al*., 2021). The adsorbed amount at time t, qt, is calculated using the intraparticle diffusion model.

$$q_t = k_{ip} t^{0.5} + C \quad (10)$$

Where intraparticle diffusion rate constant k_{ip} (mg g^{-1} $min^{0.5}$), constant C (mg g^{-1}) is related to boundary layer thickness. The graph plotted against q_t vs. t gives a non-linear line, as presented in Figure 6. If the intercept is significant, the boundary layer effect is broader. The small intraparticle diffusion constant indicates that the boundary layer has less effect on the diffusion, as shown in Table 2.

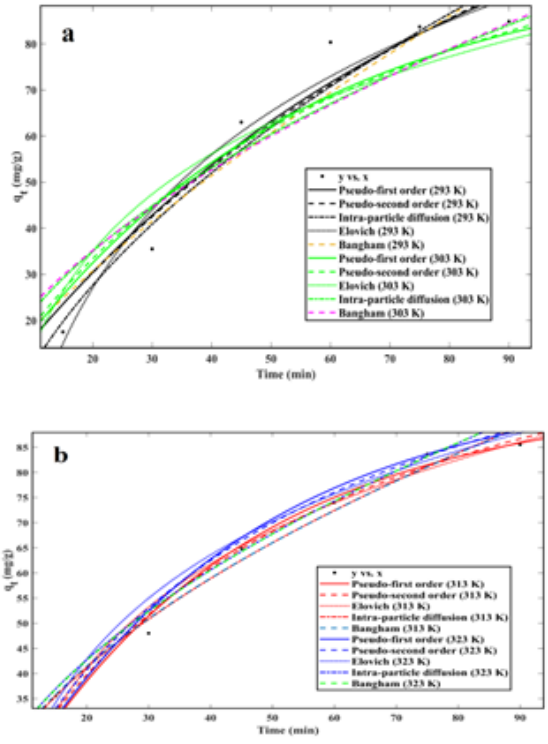

Figure 6. Kinetics for adsorption of Co(II) ions by using the TSB (a) temperature 293 & 303 K and (b) temperature 313 & 323 K

3.4.5. Elovich model

The equation of Elovich is also used to express second-order kinetics, assuming energetically solid heterogeneous adsorbent surfaces (Karthik *et al*., 2019). The following is the Elovich equation:

$$q_t = (1+\beta_E)\ln(1+\alpha_E\beta_E t) \quad (11)$$

Where α_E and β_E are elovich constants, the plot of q_t vs. t is shown in Figure 6. The plot of q_t vs. t is shown in the figure. The correlation coefficient (R^2) between 0.9589 to 0.977 for Co(II) ions is represented in Table 2. α_E the value rises with an increase in temperature. This model is not well-fitted, so the adsorption of Co(II) ions using tamarind seeds biochar follows the chemisorption process.

3.5. Adsorption thermodynamics

The approval procedure for spontaneity is based on a thermodynamic analysis of the adsorption process. Thermodynamics for adsorption was studied to evaluate the physical or chemical adsorption mechanism. The Van't Hoff equation helps to determine the thermodynamic parameters (ΔG°, ΔH°, ΔS°) for the Co(II) ions adsorption (Karthik et al., 2019). The following is the relationship between the parameters:

$$\Delta G^\circ = \Delta H^\circ - T\Delta S^\circ \quad (12)$$

Van't Hoff equation is expressed as follows

$$\ln K_c = \frac{-\Delta H^\circ}{RT} + \frac{\Delta S^\circ}{R} \quad (13)$$

Where the change in enthalpy is ΔH°, the equilibrium constant (dimensionless) is K_c, and the change in entropy is ΔS°. ΔH°, K_c, and ΔS° it is calculated by using the intercept and slope of the equation. Gibb's free energy is calculated directly from equation 12 (Figure 7).

Table 2 Kinetics constants for the adsorption of Co(II) with TSB

Kinetic model	Parameters	Temperature (K)			
		323	**313**	**303**	**293**
Pseudo-first order	q_e (mg/g)	130.4	98.51	95.01	98.14
	k_1 (min^{-1})	0.01327	0.02132	0.02598	0.0255
	R^2	0.9439	0.9794	0.9793	0.9593
Pseudo-second order	q_e (mg/g)	217.6	143.1	130.9	134.3
	k_2 (g/mg min)	0.0001	0.0001	0.0002	0.0002
	R^2	0.9692	0.9836	0.9842	0.9713
Elovich	α_E (mg/g min)	0.09535	0.1582	0.1975	0.2095
	β_E (g/mg)	18.15	13.21	12.98	12.98
	R^2	0.9589	0.9669	0.977	0.963
Bangham	k_r	3.321	6.122	9.055	9.385
	m	1.347	1.714	1.969	1.979
	R^2	0.9151	0.9828	0.9826	0.9587
Intra particle diffusion	K_{ip} (mg/g $min^{1/2}$)	13.17	9.789	9.543	9.641
	d	31.3	8.808	1.473	0.3797
	R^2	0.9401	0.9818	0.9829	0.9683

Table 3 Thermodynamic property of Co(II) ions adsorption by using TSB

Temperature (K)	ΔG° (KJ mol^{-1})	ΔH° (KJ mol^{-1})	ΔS° (KJ mol^{-1})
293	-2.7548	-65.8087	-0.2055
303	-1.138		
313	-0.3751		
323	-0.0925		

Table 3 shows the value of thermodynamic parameters for Co(II) ions at four various temperatures. The Δ*G*° value is negative for every temperature resulting in spontaneous adsorption. In the same way, the ΔH°, value is positive for all temperatures so that the adsorption process is endothermic (Sahmoune, 2019). The ΔS° positive value gives the arrangement of Co(II) ions molecules on the TSB more randomness as the temperature increases from 20 to 50 °C. Here temperature increase leads to an equilibrium constant increase. This process describes that the rate of adsorption increases when increasing in temperature (Ünlü and Ersoz, 2006). The enthalpy and entropy values for the Co(II) ions adsorption indicate the endothermic reaction, representing the chemisorption process (Demirbaş, 2003).

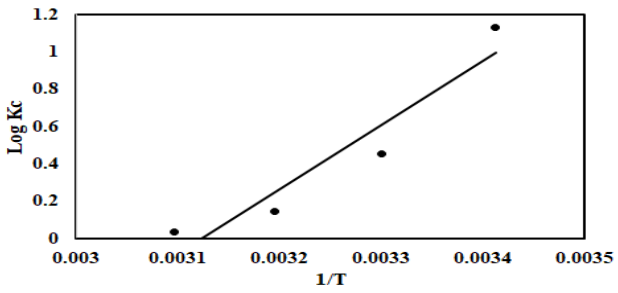

Figure 7. Thermodynamic study for Co(II) ions adsorption by using TSB

4. . Conclusion

Due to its high surface area and porosity, it is a promising adsorbent material for removing heavy metals from wastewater. The results showed that the biochar had a high surface area and porosity, which made it an effective adsorbent for Co (II) ions. The optimal conditions for Co (II) adsorption were at pH 9.0, 50 °C, 90 min, and 0.14 g/L. The isotherm results from the experimental data followed the Langmuir isotherm, indicating a monolayer adsorption mechanism for Co (II) ions. The kinetic studies showed that the Pseudo-second order kinetic model best fitted the data, indicating that the adsorption process was chemisorption. The biochar exhibited a chemisorption mechanism for Co (II) ions, with the highest adsorption capacity of 343.5 mg/g. The thermodynamic studies showed that the adsorption process was spontaneous and endothermic, indicating an efficient process for removing Co (II) ions from wastewater.

Overall, the findings of this study suggest that biochar produced from tamarind seeds by acid pyrolysis is a superior adsorbent material for removing toxic Co (II) ions from wastewater. It is a cost-effective and sustainable solution for wastewater treatment, as tamarind seeds is an abundant agricultural waste product. This study highlights the potential of biochar as an adsorbent material for heavy metal removal, which could have significant implications for environmental remediation efforts.

Conflict of Interest

The authors declare no conflict of interest.

References

Abdelbasir S.M., El-Shewaikh A.M., El-Sheikh S.M. and Ali O.I. (2021). Novel modified chitosan nanocomposites for Co (II) ions removal from industrial wastewater, *Journal of Water Process Engineering*, **41**, 102008.

Agarwal M. and Singh K. (2017). Heavy metal removal from wastewater using various adsorbents: a review, *Journal of Water Reuse and Desalination*, **7**(4), 387–419.

Akshitha V., Balakrishna K., Hegde P. and Udayashankar H.N. (2022). Evaluation of heavy metal contamination and human health risk using geo-statistical techniques in selected shallow hard rock aquifers of southwest India, *Groundwater for Sustainable Development*, **19**, 100812.

Al-Abcha A., Wang L., Reilly M. and Rosenman K. (2021). Work-related asthma in cobalt-exposed workers, *Journal of Asthma*, **58**(8), 1032–1041.

Asaithambi P., Govindarajan R., Yesuf M.B., Selvakumar P. and Alemayehu E. (2020). Enhanced treatment of landfill leachate wastewater using sono (US)-ozone (O3)–electrocoagulation (EC) process: role of process parameters on color, COD and electrical energy consumption. *Process Safety and Environmental Protection*, **142**, 212–218.

Asaithambi P., Govindarajan R., Yesuf M.B., Selvakumar P. and Alemayehu E. (2021). Investigation of direct and alternating current–electrocoagulation process for the treatment of distillery industrial effluent: Studies on operating parameters. *Journal of Environmental Chemical Engineering*, **9**(2), 104811.

Azam K., Shezad N., Shafiq I., Akhter P., Akhtar F., Jamil F., Shafique S., Park Y.K. and Hussain M. (2022). A review on activated carbon modifications for the treatment of wastewater containing anionic dyes, *Chemosphere*, 135566.

Banu J.R., Merrylin J., Kavitha S., Kannah R.Y., Selvakumar P., Gopikumar S., Sivashanmugam P., Do K.U. and Kumar G. (2021). Trends in biological nutrient removal for the treatment of low strength organic wastewaters. *Current Pollution Reports*, **7**(1), 1–30.

Bhairappa A., Konka S. and Lade R. (2020). Iron Adsorption from Textile Industrial Effluent on Activated Carbon Prepared from Tamarind Seeds (Tamarindus indica L.).

Bordoloi N., Goswami R., Kumar M. and Kataki R. (2017). Biosorption of Co (II) from aqueous solution using algal biochar: kinetics and isotherm studies, *Bioresource technology*, **244**, 1465–1469.

Chen H., Chen X., Qiao Z. and Liu H. (2016). Release and transformation behavior of Cl during pyrolysis of torrefied *rice straw, Fuel*, **183**, 145–154.

Demirbaş E. (2003). Adsorption of cobalt (II) ions from aqueous solution onto activated carbon prepared from hazelnut shells, *Adsorption Science & Technology*, **21**(10), 951–963.

Ekrami E., Pouresmaieli M., sadat Hashemiyoon E., Noorbakhsh N. and Mahmoudifard M. (2022). Nanotechnology: a sustainable solution for heavy metals remediation, *Environmental Nanotechnology, Monitoring & Management*, **18**, 100718.

Güçoğlu M. and Şatıroğlu N. (2022). Adsorption of Pb (II), Cu (II), Cd (II), Ni (II), and Co (II) ions by newly synthesized 2-(2-Hydroxyphenyl) Benzothiazole-functionalized silica, *Journal of Molecular Liquids*, **348**, 118388.

Hossain N., Nizamuddin S., Griffin G., Selvakannan P., Mubarak N.M. and Mahlia T.M.I. (2020). Synthesis and characterization of rice husk biochar via hydrothermal carbonization for wastewater treatment and biofuel production, *Scientific Reports*, **10**(1), 18851.

Huang X., Liu Y., Liu S., Tan X., Ding Y., Zeng G., Zhou Y., Zhang M., Wang S. and Zheng B. (2016). Effective removal of Cr (VI) using β-cyclodextrin–chitosan modified biochars with adsorption/reduction bifuctional roles, *RSC advances*, **6**(1), 94–104.

Karthik V., Selvakumar P., Sivarajasekar N., Megavarshini P., Brinda N., Kiruthika J., Balasubramani K., Ahamad T. and Naushad M. (2020). Comparative and equilibrium studies on anionic and cationic dyes removal by nano-alumina-doped catechol formaldehyde composite, *Journal of Chemistry*, 2020.

Karthik V., Senthil Kumar P., Vo D.V.N., Selvakumar P., Gokulakrishnan M., Keerthana P., Audilakshmi V. and Jeyanthi J. (2021). Enzyme-loaded nanoparticles for the degradation of wastewater contaminants: a review. *Environmental Chemistry Letters*, **19**, 2331–2350.

Karthik V., Karuna B., Jeyanthi J. and Periyasamy S. (2022a). Biochar production from Manilkara zapota seeds, activation and characterization for effective removal of Cu2+ ions in polluted drinking water, *Biomass Conversion and Biorefinery*, 1–15.

Karthik V., Selvakumar P., Kumar P.S., Satheeskumar V., Vijaysunder M.G., Hariharan S. and Antony K. (2022b). Recent advances in electrochemical sensor developments for

detecting emerging pollutant in water environment. *Chemosphere*, 135331.

Karthik V.a., Saravanan K., Patra C., Ushadevi B., Vairam S. and Selvaraju N. (2019). 'Biosorption of acid yellow 12 from simulated wastewater by non-viable T. harzianum: kinetics, isotherm and thermodynamic studies, *International Journal of Environmental Science and Technology*, **16**(11), 6895–6906.

Kılıc M., Kırbıyık C., Çepelioğullar Ö. and Pütün A.E. (2013). Adsorption of heavy metal ions from aqueous solutions by bio-char, a by-product of pyrolysis, *Applied Surface Science*, **283**, 856–862.

Leyssens L., Vinck B., Van Der Straeten C., Wuyts F. and Maes L. (2017). Cobalt toxicity in humans—A review of the potential sources and systemic health effects, *Toxicology*, **387**, 43–56.

Medyńska-Juraszek A., Ćwieląg-Piasecka I., Jerzykiewicz M. and Trynda J. (2020). Wheat Straw Biochar as a Specific Sorbent of *Cobalt in Soil, Materials (Basel)*, **13**(11).

Murugesan S.R., Sivakumar V., Velusamy S., Ravindiran G., Sundararaj P., Maruthasalam V., Thangavel R., Ramasamy G.S., Panneerselvam M. and Periyasamy S. (2022). Biosorption of Malachite Green from Aqueous Phase by Tamarind Fruit Shells Using FBR. *Advances in Materials Science and Engineering*, 2022.

Obaideen K., Shehata N., Sayed E.T., Abdelkareem M.A., Mahmoud M.S. and Olabi A. (2022). The role of wastewater treatment in achieving sustainable development goals (SDGs) and sustainability guideline, *Energy Nexus*, **7**, 100112.

Papageorgiou S.K., Kouvelos E.P., Favvas E.P., Sapalidis A.A., Romanos G.E. and Katsaros F.K. (2010). Metal–carboxylate interactions in metal–alginate complexes studied with FTIR spectroscopy, *Carbohydrate research*, **345**(4), 469–473.

Periyasamy S., Karthik V., Senthil Kumar P., Isabel J.B., Temesgen T., Hunegnaw B.M., Melese B.B., Mohamed B.A. and Vo D.V.N. (2022). Chemical, physical and biological methods to convert lignocellulosic waste into value-added products. A review. *Environmental Chemistry Letters*, **20**(2), 1129–1152.

Periyasamy S., Isabel J.B., Kavitha S., Karthik V., Mohamed B.A., Gizaw D.G., Sivashanmugam P. and Aminabhavi T.M. (2023). Recent advances in consolidated bioprocessing for conversion of lignocellulosic biomass into bioethanol–a review. *Chemical Engineering Journal*, **453**, 139783.

Rajendran M., Ramanathan R., Ganesan P. and Shanmugavel R. (2021). Experimental analysis of tamarind seed powder-based flash powder composition for eco-friendly firecrackers, *Journal of Thermal Analysis and Calorimetry*, **143**, 3009–3021.

Roba B., Yilma M., Abay Y., Mekonnen A., Periyasamy S., Duraisamy K. and Temesgen T. (2023). A novel approach for the defluorination of groundwater using trivalent-metal hydroxide/bone-char composite adsorbent. *Urban Climate*, **47**, 101340.

Sahmoune M.N. (2019). Evaluation of thermodynamic parameters for adsorption of heavy metals by green adsorbents, *Environmental Chemistry Letters*, **17**(2), 697–704.

Saravanan A., Kumar P.S., Vo D.V.N., Jayasree R., Hemavathy R.R.V., Karthik V., Karishma S., Jeevanantham S., Manivasagan V. and George C.S. (2021). Surface improved agro-based material for the effective separation of toxic Ni (II) ions from aquatic environment, *Chemosphere*, **283**, 131215.

Shen Z., Hou D., Jin F., Shi J., Fan X., Tsang D. C. and Alessi D.S. (2019). Effect of production temperature on lead removal mechanisms by rice straw biochars, *Science of the Total Environment*, **655**, 751–758.

Shi J., Fan X., Tsang D.C., Wang F., Shen Z., Hou D. and Alessi D.S. (2019). Removal of lead by rice husk biochars produced at different temperatures and implications for their environmental utilizations, *Chemosphere*, **235**, 825–831.

Shrivastava R. and Singh N. (2022). Agro-wastes sustainable materials for wastewater treatment: Review of current scenario and approaches for India, Materials Today: Proceedings.

Sikiru S., Ayodele O.A., Sanusi Y.K., Adebukola S.Y., Soleimani H., Yekeen N. and Haslija A.A. (2022). A comprehensive review on nanotechnology application in wastewater treatment a case study of metal-based using green synthesis, *Journal of Environmental Chemical Engineering*, 108065.

Silva C.P., Jaria G., Otero M., Esteves V.I. and Calisto V. (2018). Waste-based alternative adsorbents for the remediation of pharmaceutical contaminated waters: Has a step forward already been taken?, *Bioresource Technology*, **250**, 888–901.

Sithara R., Selvakumar P., Arun C., Anandan S. and Sivashanmugam P. (2017). Economical synthesis of silver nanoparticles using leaf extract of Acalypha hispida and its application in the detection of Mn (II) ions. *Journal of advanced research*, **8**(6), 561–568.

Teschke R. (2022). Aluminum, Arsenic, Beryllium, Cadmium, Chromium, Cobalt, Copper, Iron, Lead, Mercury, Molybdenum, Nickel, Platinum, Thallium, Titanium, Vanadium, and Zinc: Molecular Aspects in Experimental Liver Injury, *International Journal of Molecular Sciences*, **23**(20), 12213.

Ünlü N. and Ersoz M. (2006). Adsorption characteristics of heavy metal ions onto a low cost biopolymeric sorbent from aqueous solutions, *Journal of hazardous materials*, **136**(2), 272–280.

Velusamy K., Periyasamy S., Kumar P.S., Vo D.V.N., Sindhu J., Sneka D. and Subhashini B. (2021a). Advanced techniques to remove phosphates and nitrates from waters: a review. *Environmental Chemistry Letters*, **19**, 3165–3180.

Velusamy K., Periyasamy S., Kumar P.S., Jayaraj T., Krishnasamy R., Sindhu J., Sneka D., Subhashini B. and Vo D.V.N. (2021b). Analysis on the removal of emerging contaminant from aqueous solution using biochar derived from soap nut seeds. *Environmental Pollution*, **287**, 117632.

Velusamy K., Periyasamy S., Kumar P.S., Rangasamy G., Pauline J.M.N., Ramaraju P., Mohanasundaram S. and Vo D.V.N. (2022). Biosensor for heavy metals detection in wastewater: A review. *Food and Chemical Toxicology*, 113307.

Wang R., Deng L., Fan X., Li K., Lu H. and Li W. (2021). Removal of heavy metal ion cobalt (II) from wastewater via adsorption method using microcrystalline cellulose–magnesium hydroxide, *International Journal of Biological Macromolecules*, **189**, 607–617.

Wu Q., Xian Y., He Z., Zhang Q., Wu J., Yang G., Zhang X., Qi H., Ma J., Xiao Y. and Long L. (2019). Adsorption characteristics of Pb(II) using biochar derived from spent mushroom substrate, *Scientific Reports*, **9**(1), 15999.

Zhu Q., Liao S., Lu X., Shi S., Gong D., Cheang I., Zhu X., Zhang H. and Li X. (2021) Cobalt exposure in relation to cardiovascular disease in the United States general population, *Environmental Science and Pollution Research*, **28**(31), 41834–41842.